JGR Oceans

RESEARCH ARTICLE

Key Points:
- Subseasonal variability accounts for a substantial fraction of the Florida Current transport variance
- Coastal-trapped waves are the primary source of the subseasonal variability in the Florida Current
- Alongshore wind-driven Ekman dynamics control the genesis of the subseasonal coastal-trapped waves

Author Contributions:
Conceptualization: Kandaga Pujiana
Data curation: Denis L. Volkov, Ryan H. Smith, Rigoberto Garcia
Formal analysis: Kandaga Pujiana, Denis L. Volkov, Shenfu Dong, Gustavo Goni
Funding acquisition: Denis L. Volkov, Shenfu Dong, Gustavo Goni, Molly Baringer
Investigation: Kandaga Pujiana
Methodology: Kandaga Pujiana
Software: Kandaga Pujiana
Visualization: Kandaga Pujiana
Writing – original draft: Kandaga Pujiana
Writing – review & editing: Kandaga Pujiana, Denis L. Volkov, Shenfu Dong, Gustavo Goni, Molly Baringer, Ryan H. Smith

Genesis of the Gulf Stream Subseasonal Variability in the Florida Straits

Kandaga Pujiana[1,2], Denis L. Volkov[1,2], Shenfu Dong[2], Gustavo Goni[2], Molly Baringer[2], Ryan H. Smith[2], and Rigoberto Garcia[1,2]

[1]University of Miami Cooperative Institute for Marine and Atmospheric Studies, Miami, WA, USA, [2]NOAA Atlantic Oceanographic and Meteorological Laboratory, Miami, WA, USA

Abstract The properties and generation mechanisms of the Florida Current on the subseasonal timescale (20–100 days) are evaluated from in-situ and satellite observations. The Florida Current volume transport estimates from submarine cable measurements reveal that subseasonal variability accounts for 37% of the total transport variance and is most variable from September to November. Here we show that coastal-trapped waves are the primary driver of the subseasonal variability in the Florida Current transport. The role of local winds and open ocean signals is of secondary importance. The alongshore wind component of the anomalous North Atlantic subtropical anticyclone generates the subseasonal coastal-trapped waves off the northern South Atlantic Bight coast. The subseasonal coastal-trapped waves propagate from Cape May to Apalachicola, behaving as Kelvin waves in the Florida Straits and as continental shelf waves along the rest of the waveguide. They affect the Florida Current transport by up to 2.6 Sv, on average. As the subseasonal waves propagate into the Gulf of Mexico, their energy substantially dissipates. The wave amplitude at Port Canaveral of up to 15 cm is three times higher than at Apalachicola. Concurrent subseasonal changes of the meridional overturning circulation in the subtropical North Atlantic are discussed.

Plain Language Summary The Florida Current, an important constituent of the meridional overturning circulation in the subtropical North Atlantic, is crucial for the oceanic heat and freshwater transports and thereby influences the regional weather and climate variations. Past studies show that the Florida Current exhibits changes with time scales that range from days to years. Our study attempts to elucidate the energetic subseasonal variability of the Florida Current with periods ranging from 20 to 100 days, whose characteristics and genesis have remained least understood. Based on the analyses of the most extensive in-situ and satellite measurements in the Florida Straits, we demonstrate that coastally trapped waves originating from the northern South Atlantic Bight are the predominant driver of the subseasonal variability in the Florida Current. The alongshore wind-forced subseasonal waves modulate the Florida Current transport substantially. The far-reaching impacts of the waves on sea level along the United States East and Gulf Coast and concurrent subseasonal changes of the overturning circulation are discussed.

1. Introduction

The Florida Current (FC), the headwaters of the Gulf Stream, is an important component of the meridional overturning circulation in the subtropical North Atlantic. It is a highly variable, surface-intensified flow, with variations spanning a broad range of timescales from days to years (e.g., Beal et al., 2008; Lee et al., 1985; Meinen et al., 2010; Schott et al., 1986). The FC has been monitored nearly continuously since 1982 using a submarine telephone cable between Florida and the Bahamas (inset of Figure 1) (e.g., Baringer & Larsen, 2001). Calibrated with direct ocean current velocity measurements from Pegasus and dropsonde profilers, the cable voltages yield the daily time series of the FC volume transport (Garcia & Meinen, 2014). The long-term average cable-derived transport and its standard deviation value during 1982–2020 are 31.8 ± 3.4 Sv [1 Sv = 10^6 m^{3}s^{-1}], reasonably consistent with the FC transport estimates documented in previous studies (Baringer & Larsen, 2001; Larsen & Smith, 1992; Meinen et al., 2010).

About 30% of the observed FC transport variance is attributable to processes with a climate-relevant timescale range between seasonal and longer periods (e.g., Meinen et al., 2010). The seasonal cycle of the FC transport exhibits a maximum in July, followed by a quick drop to a minimum in November - December, with a peak-to-peak range of 4–5 Sv changing with time (Baringer & Larsen, 2001; Larsen & Smith, 1992; Rosenfeld
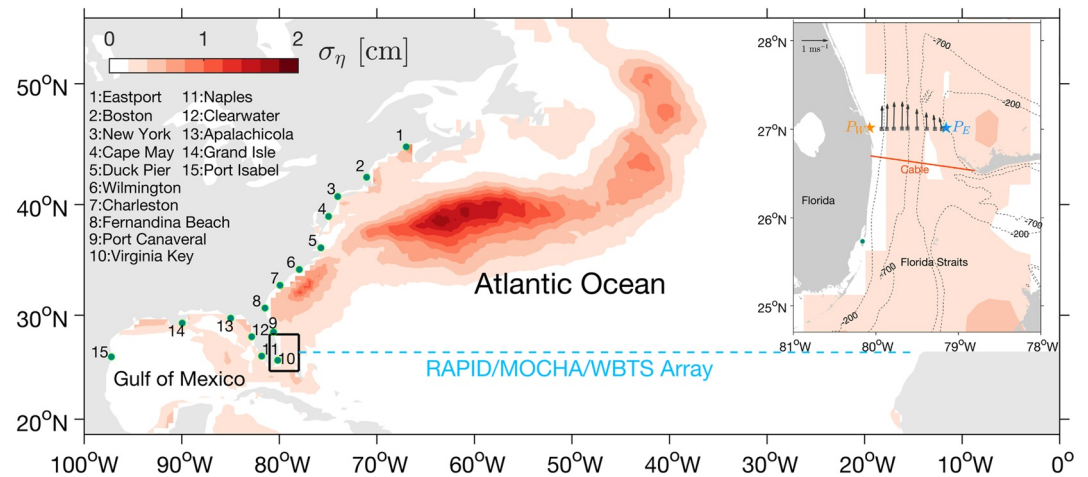
Figure 1. Standard deviation of the satellite-derived sea surface height anomaly (η; shading) in the subseasonal period band between 20 and 100 days in the North Atlantic, based on the data observed during 2001–2019. Green dots mark a network of tide gauges along the U.S. East and Gulf Coast. The blue dashed line marks the location of the Rapid climate change/Meridional overturning circulation and heat flux array/Western Boundary Time Series (RAPID/MOCHA/WBTS) array. The inset illustrates locations of the observations in the Florida Straits, with stars marking bottom pressure recorders, gray boxes denoting dropsonde, Pegasus, lowered Acoustic Doppler Current Profiler (ADCP), eXpendable BathyThermograph (XBT), and Conductivity-Temperature-Depth (CTD) casts, arrows indicating the vertical-mean of horizontal velocity averaged for all the casts between 2001 and 2019, and the red line showing submerged cable for monitoring the FC transport. Dashed contours indicate bottom depth.

et al., 1989). The driving mechanisms of the seasonal cycle have been attributed to barotropic processes in response to winds prevailing either locally in the Florida Straits or off the Northeast coast of North America. The solutions of a wind-forced response model indicate that the seasonal cycle of the FC is a barotropic response to the along-stream winds within the Straits (Lee & Williams, 1988). In contrast, the results of an adjoint model link the annual cycle to wind-forced barotropic waves originating along the Northeast American coast (Czeschel et al., 2012). As for the year-to-year change of the FC transport, Domingues et al. (2016) proposed long baroclinic Rossby waves originating in the eastern North Atlantic as a mechanism modulating the FC seasonal change. DiNezio et al. (2009) suggested a similar FC transport interannual variability source.

Most of the observed FC transport variance lies between the tidal and seasonal periods with amplitudes comparable to or greater than the seasonal cycle (Meinen et al., 2010; Mooers et al., 2005; Schott et al., 1988). Many studies have reported a variety of processes governing the FC transport fluctuations on synoptic or weather timescales from a few to 15 days (e.g., Johns & Schott, 1987; Lee & Williams, 1988). Synoptic-scale winds over the Florida Straits, which are more energetic during winter than summer, contribute substantially to forcing the 4–10 days variations of the FC transport (Schott et al., 1988). Synoptic changes in the FC often reflect a geostrophic response to the sea level gradient change across the Florida Straits. They derive from the convergence of cross-strait current driven by synoptic along-strait winds via Ekman dynamics (Lee & Williams, 1988). As for the 10–15-day periods, the FC is dominated by northward propagating features reminiscent of meanders. Nevertheless, the impacts of meandering motions on the FC transport are limited as they predominantly project in the cross-strait direction (Johns & Schott, 1987).

The broad period range between the synoptic and seasonal timescales is the subseasonal or intraseasonal period band, which conventionally encompasses a range of periods between 20 and 100 days (e.g., Maloney et al., 2008). The FC transport exhibits energetic variability within the subseasonal period band. Using a record between 1982 and 2007, Meinen et al. (2010) showed that 46% of the FC transport variance is attributable to the variability between 1-to-11 months. Volkov et al. (2020), using altimetry during 2005–2020, demonstrated that the FC transport variability for the 20–170 days band exhibits a standard deviation of 2.4 Sv, larger than that for the seasonal and interannual period bands.

Despite its substantial contribution to the highly variable FC (Meinen et al., 2010), the evolution and genesis of subseasonal variability in the Florida Straits remain not fully understood. Schott et al. (1988) attempted to analyze

the subseasonal variability based on ocean current velocities from an array of moorings across the Florida Straits near the submarine cable from April 1982–June 1984. They reported a correlation between the FC volume transport and local winds varying on timescales ranging between a couple of days to 3 months. They argued that a simple frictional flow model driven by the along-strait winds could explain the correlation, implying local winds as a likely source of the subseasonal variability. Besides the local winds, mesoscale eddies from the east of the Bahamas may force the subseasonal variability in the FC. Frajka-Williams et al. (2013) argued that eddies are a dominant control for the Antilles Current fluctuations and may influence the FC variations on timescales longer than 50 days.

Due to the key role in transporting heat, freshwater, and nutrients, improving our understanding of the FC variations at a wide range of timescales is critical. This study builds upon previous investigations to evaluate the characteristics and mechanisms of the FC transport variations on the subseasonal timescale between 20 and 100 days in terms of coastal-trapped wave theory. Plausible impacts of subseasonal local winds and remote signals from the interior of the North Atlantic on the FC transport are reassessed. In addition to the subseasonal fluctuations in the FC transport, we also examine concurrent changes of other components in the meridional overturning circulation (MOC) in the subtropical North Atlantic during pronounced subseasonal wave events.

This manuscript is organized as follows. In Section 2, we describe the data and methods. Section 3 discusses the main properties of subseasonal variability in the oceanic parameters observed in the Florida Straits and how they relate to local winds and eddies and Rossby waves from the open ocean. Then, in Section 4, we assess inferences of subseasonal coastal-trapped waves from sea level anomaly along the United States (U.S) East and Gulf Coast and their impact on the FC transport. Section 5 examines the basin-scale changes in the wind field and MOC evolution associated with the subseasonal wave events. A discussion (Section 6) and conclusions (Section 7) follow.

2. Data and Methods

To assess the subseasonal variability in the FC transport, we utilize the most extensive observations to date in the Florida Straits. The daily, quasi-continuous volume transport estimates from the undersea telephone cable in the Florida Straits at 27°N (red line in the inset of Figure 1) from 1982 to 2019 are the primary data from which we derived the inferences for the subseasonal variability in the FC. The tidal and magnetic field variations were removed from the daily FC transport estimates using a 3-day low pass filter (Meinen et al., 2010). The transport estimates from repeated shipboard sections at 27°N (Garcia & Meinen, 2014) and along-track satellite altimetry measurements across the Florida Straits (Volkov et al., 2020) were also examined. The ship sections include Pegasus, dropsonde, and lowered Acoustic Doppler Current Profiler (LADCP) casts at nine stations (marked by rectangles in the inset of Figure 1).

Despite showing an overall good agreement with the shipborne measurements, the accuracy of the cable's estimates was relatively low between 1993 and 1998, when the cable was in active use for telecommunication services (Larsen, 1991; Volkov et al., 2020). Following this period, there was a 17-month data gap in the cable record. Therefore, we examined the FC transport estimates between 2001 and 2019. A subset of the FC transport time series from different measurement techniques is shown in Figure 2a.

Besides the FC transport estimates, we examined pressure data from two bottom pressure recorders (BPRs) deployed in shallow waters (~12 m) on the western and eastern sides of the Florida Straits at 27°N (stars in the inset of Figure 1; Meinen et al., 2021). We hereafter refer to the pressure measured by the BPRs on the western and eastern sides of the Florida Straits as P_W and P_E, respectively. For this study, we examined the daily averages of the 5-min average pressure records between July 2008–September 2014 (Figure 2b), during which both BPRs were synchronously operational and recorded nearly continuous data. The 5-min average data were smoothed with a 3-day low-pass filter and then daily averaged to remove the tides (Meinen et al., 2021).

Along with the dropsonde and LADCP casts, the shipboard surveys across the FC at 27°N also included Conductivity-Temperature-Depth (CTD) and eXpendable BathyThermograph (XBT) deployments, with the former measuring profiles of both temperature (T) and salinity (S), and the latter profiling only T. The World Ocean Atlas 2013 (WOA2013) salinity product was used to supplement T measured with XBT deployments. We used the subsurface T and derived Brunt-Väisällä frequency (N) profiles to assess the subseasonal coastal-trapped wave properties, including their vertical and horizontal (cross-shelf) scales. The stratification frequency was
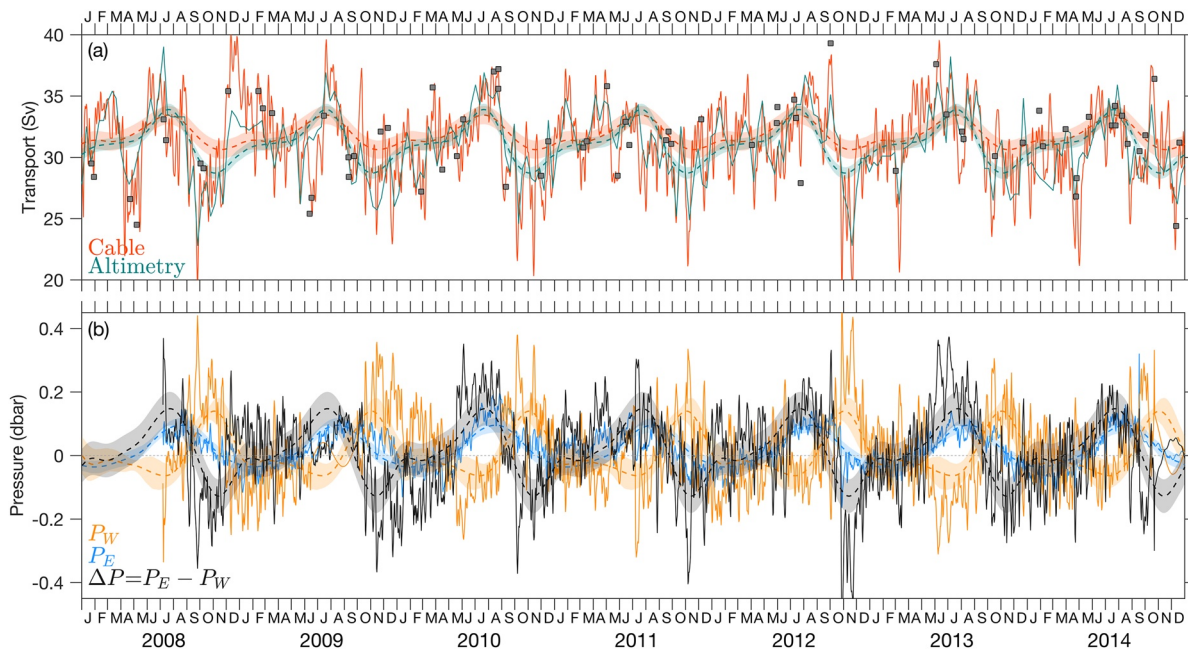
Figure 2. (a) A subset of the FC volume transport time series estimated from cable voltages (red), satellite altimetry (green), and shipboard measurements (dropsondes and lowered Acoustic Doppler Current Profiler) (rectangles). (b) Time series of pressure data from the bottom pressure recorders deployed on the west side (P_W; orange) and east side (P_E; blue) of the Florida Straits. The black curve indicates the across-channel or cross-stream pressure difference [$\Delta P = P_E - P_W$]. The color-coded dashed curves denote the seasonal cycles attributable to the time series, with shades indicating the cycles' 95% bootstrap confidence limits.

determined from the observed potential density (ρ) profiles, expressed as $N^2 \equiv \frac{-g}{\rho_0} \frac{d\rho}{dz}$, where ρ was computed from T and S, ρ_0 is the background density structure inferred from the time-averaged ρ, z is the vertical coordinate, and g is the gravitational acceleration constant of 9.8 m s^{-2}.

In addition to the in-situ observations in the Florida Straits, we examined daily sea level anomaly records during 2001–2019 from a network of tide gauges along the U.S. East and Gulf Coast (green dots in Figure 1). The tide gauge data used in this study is provided by the University of Hawaii Sea Level Center (UHSLC) (Caldwell et al., 2015). The isostatic response to surface atmospheric pressure was removed from the tide gauge data using fields of the inverted barometer effect (Piecuch & Ponte, 2015; Ponte, 2006) estimated from sea level pressure data provided by the National Centers for Environmental Prediction (NCEP) Reanalysis-2 (Kanamitsu et al., 2002). We also analyzed satellite-derived wind stress (τ) and sea surface height data over the North Atlantic to gain insights into non-local processes driving the FC subseasonal variability and their basin-scale structures. We employed the daily, 0.25° latitude x 0.25° longitude gridded τ and sea surface height datasets for the 2001–2019 period from the Copernicus Marine and Environment Monitoring Service (CMEMS) products. The anomalies of the tide-gauge sea level and altimetry sea surface height are henceforth referred to as η.

The FC transport measurements serve as a western boundary endpoint of a subtropical MOC and heat transport monitoring system at about 26.5°N. The system is known as the Rapid climate change/Meridional overturning circulation and heat flux array/Western Boundary Time Series (RAPID/MOCHA/WBTS) program (e.g., McCarthy et al., 2015). The MOC transport is obtained as the sum of the upper mid-ocean (UMO) transport in the upper ~1,100 m between the Bahamas and Africa, the near-surface meridional Ekman (EK) transport, and the FC cable transport (e.g., Frajka-Williams et al., 2019). We used the 12-hourly estimates of the EK, UMO, and MOC transports in 2004–2019 to explore how they are affected by the subseasonal fluctuations in the FC transport. The 12-hourly transport estimates were smoothed with a 3-day low-pass filter and then daily averaged.

Some time series and spatial analysis methods were applied to the in-situ and satellite data. We analyzed the 20–100 days band-pass filtered data to assess the spatial structures of the subseasonal mode using a Complex Empirical Orthogonal Function (CEOF) analysis and a linear regression method (Thomson & Emery, 2014). Isolating the variability of the subseasonal and other frequency bands was achieved using a fourth-order band-pass Butterworth filter. Any data gaps were filled with a simple linear interpolation. To estimate the alongshore
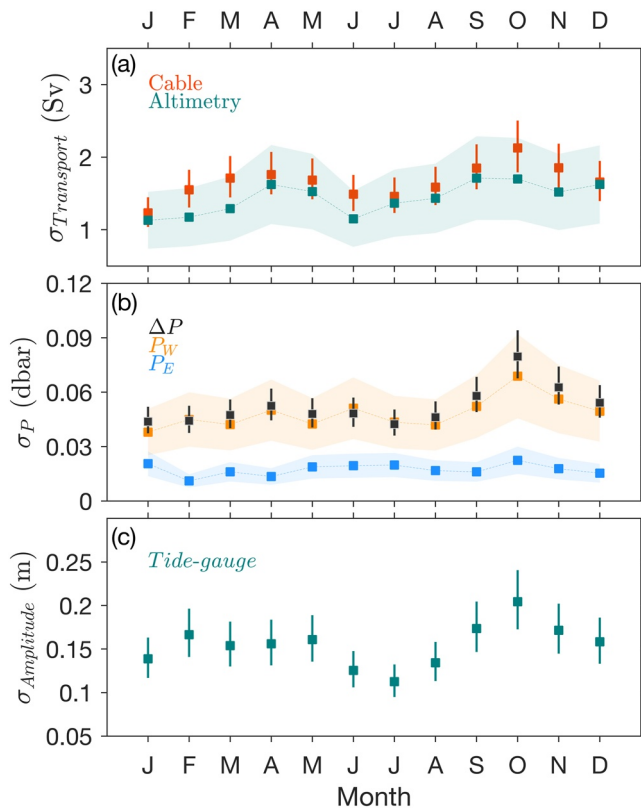
Figure 3. The seasonal cycle of the standard deviation of the subseasonal variations of (a) the FC transport estimates, (b) the bottom pressure records in the Florida Straits, and (c) the principal component of the leading Complex Empirical Orthogonal Function mode of the η fluctuations at tide gauges along the U.S. East and Gulf Coast between Cape May and Apalachicola. Color-coded shadings or vertical lines denote 95% bootstrap confidence limits. The standard deviations observed between 2001 and 2019 are used to determine the seasonal cycle for the FC transport and the tide gauge η data, while those throughout July 2008–September 2014 are employed for the bottom pressure data.

wavenumbers of subseasonal coastal-trapped waves, we applied a coherence analysis (Percival & Walden, 1993) to the coastal η data from multiple pairs of tide gauges. Based on the phase lags determined from the coherence analysis, we derived the wavenumbers, which were then used to estimate the dispersion relation of the subseasonal mode. We employed a wavelet coherence analysis to gauge a plausible covariance and its evolution over a continuous time-frequency space between the FC transport and local winds and open ocean signals (Grinsted et al., 2004).

3. Subseasonal Variability in the Florida Straits

3.1. Statistical Inferences

Consistent with the results reported in past studies (e.g., Baringer & Larsen, 2001; Meinen et al., 2010), the FC volume transport inferred from cable voltages reveals large variations about its poleward transport, with the mean and standard deviation values of 31.6 ± 3.3 Sv for the entire record analyzed herein between 2001 and 2019 and of 31.1 ± 3.4 Sv for the subset throughout 2008–2014 as shown in Figure 2a. For comparison, the mean and standard deviation estimates from altimetry are 31.2 ± 2.8 Sv during 2001–2019 and 31.0 ± 2.8 Sv during 2008–2014. Ubiquitous subseasonal and synoptic variations characterize the FC transport estimates (Figure 2a).

A quasi-monthly oscillation predominantly accounts for the subseasonal variability of the FC transport observed during 2001–2019, while oscillations every 2–3 months prevail in some years, including between 2008 and 2014 (Figure 2a). The standard deviation of the subseasonal variability observed between 2001 and 2019 from the cable is 1.69 Sv. Schott et al. (1988), based on earlier observations of moored current meter arrays between 1982 and 1984 in the Florida Straits, revealed a rather red spectrum of the FC transport across the resolved frequencies, indicative of no particular dominant frequency within the subseasonal frequency band. The discrepancy may stem from less variable subseasonal variation occurring in that specific period reported in their study. Intermittent subseasonal signature is not atypical in oceanic and atmospheric processes (Lau & Waliser, 2011). Indeed, the voltage-derived FC transport confirms an overall smaller standard deviation, 1.53 Sv, from 1982 to 1984.

Subseasonal variability contains a significant fraction of the total variance of the FC transport variations. The total variance during 2001–2019 is 10.7 Sv^2, with the subset between 2008 and 2014 exhibiting a larger value of 11.6 Sv^2. Of the total FC transport variability, about 37% of the variance is attributable to subseasonal variability for the entire data or the subset. It is higher than the total percentage of the synoptic (3–15 days), seasonal (11–13 months), and interannual variances (13–42 months), which are 25%, 2%, and 8%, respectively. Relative to the 20-day low-pass filtered FC transport anomalies (seasonal cycle removed), subseasonal fluctuation accounts for 62% of the transport anomalies during 2001–2019. The percentage slightly increases to 67% when considering the data between 2008 and 2014.

Subseasonal variability constitutes a significant fraction of the total pressure variance in the Florida Straits. The total percentage of subseasonal variance for P_W, P_E, and ΔP is 24%, 16%, and 24%, respectively, comparable to or higher than the total percentage of the synoptic and seasonal variances. Moreover, subseasonal variability notably contributes to the 20-day low-pass filtered pressure anomalies with the seasonal cycle removed. It accounts for 50%, 37%, and 37% of the total variance of the low-pass filtered P_W, P_E, and ΔP anomalies, respectively. The discrepancy in the percentage confirms a more energetic subseasonal signature on the west side of the Florida Straits.

Subseasonal variability in the Florida Straits exhibits seasonality. The subseasonal variation in the FC transport is more variable during September - November, and peaks in October (Figure 3a). A more energetic subseasonal

variability in autumn is consistently observed in the FC transport estimates from both the cable and altimetry. Similar to the transport estimates, the pressure on the west side and the cross-stream pressure gradient on the subseasonal timescale demonstrate a maximum standard deviation in October (Figure 3b).

Besides being the most variable in boreal autumn, the FC transport and the bottom pressure on the subseasonal timescale are statistically correlated. The FC transport is correlated with ΔP, with a correlation coefficient $r = 0.71$ (0.69, 0.73), where the values in the bracket represent 95% confidence limits based on Fisher's z transformation. When only the autumn months data are considered, the r-value increases to 0.84 (0.81, 0.87). The correlation suggests that a linear relationship between the pressure difference and the FC transport would explain about 50% (70% for the autumn data) of the FC transport variance for the subseasonal band. The pressure on the western side of the Florida Straits dominates the subseasonal geostrophic FC variability, with about 41% (70% for the autumn time series) of the FC transport subseasonal variance being accounted for by P_W. Meanwhile, P_E accounts for only 16% of the FC transport subseasonal variance, even when solely based on the autumn data.

3.2. Influence of Local Winds and Open Ocean Signals

To trace energy sources for the subseasonal variations of the FC transport estimates and the pressure records, we first review the potential impact of local winds in the Florida Straits. Schott et al. (1988), using two-year-long transport estimates from an array of current meters deployed in the vicinity of the cable during 1982–1984, argued that the FC transport and local winds exhibit a degree of coherence over a broad period band from a few days to a couple of months. The coherence is particularly evident between the along-channel wind and the FC transport for periods shorter than 30 days.

Our assessment employing more extended datasets during 2001–2019 suggests that local winds are not a major factor in driving the subseasonal variability of the FC transport. A lagged correlation analysis indicates that the wind stress components do not strongly correlate with the FC transport and bottom pressure on the subseasonal timescale. The meridional wind stress (τ^y) demonstrates the strongest correlation with both the FC transport [$r = 0.21$ (0.16, 0.23)] and ΔP [$r = 0.28$ (0.22, 0.30)], with τ^y leading by 1–2 days. The zonal wind stress (τ^x) and wind stress curl ($\nabla \times \tau$) show weaker correlations.

Despite exhibiting an overall weak correlation, τ^y and the FC transport are coherent for some periods of the subseasonal band. The subseasonal variations of the two parameters exhibit the largest squared coherence values for periods between 20 and 30 days, consistent with the results of Schott et al. (1988), but the coherent signals occur intermittently throughout the observational period between 2001 and 2019. For example, the 20–30 days variations for the data subset between 2003 and 2006 were significantly coherent only between February–April 2005 and August–September 2006 (Figure 4). Although significant, the coherent signals observed in February - April 2005 do not show a phase relationship supportive of a causal relationship between the wind and the FC transport. The phase suggests that the latter leads the former (arrows in Figure 4). This unfavorable phase relationship and sporadic coherence throughout the observational period likely explain the overall weak correlation between the two.

As both the FC transport and the pressure gradient show a weak positive correlation with τ^y, a balance between wind stress and frictional dissipation in the along-stream direction is not a predominant factor in explaining the
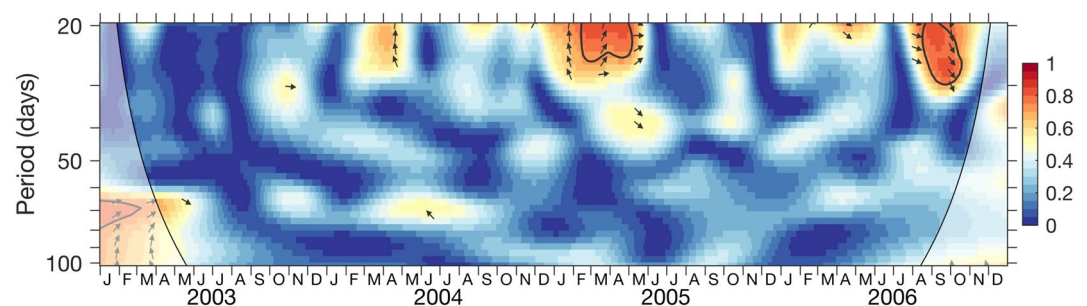
Figure 4. The values of squared wavelet coherence between the subseasonal variations of the τ^y and the FC transport during 2003–2006. Arrows denote the phase lag, with those pointing right and down indicating an in-phase relationship and the wind leading the transport by 90°, respectively. The magnitude-squared wavelet coherence significant at the 95% significance level is contoured. The blurred area marks the edge effects in the coherence data.
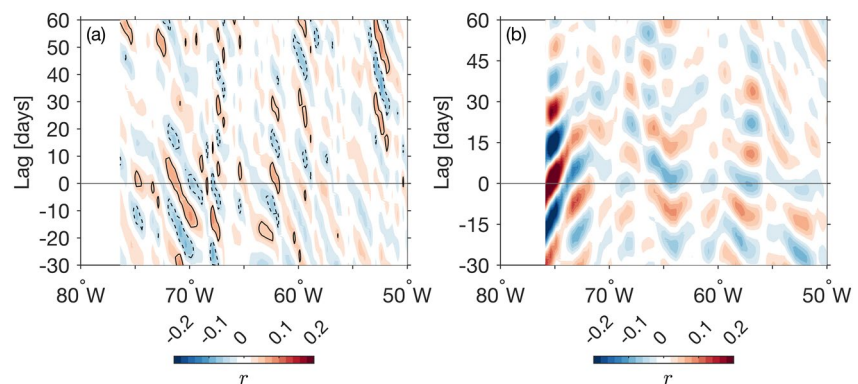
Figure 5. (a) Lagged correlation coefficients [r] between the subseasonal variations of the FC transport and satellite η averaged at latitudes between 26 and 27°N. (b) The correlation coefficients between the subseasonal variations of tide gauge η at Duck Pier and satellite η averaged at latitudes between 34 and 36°N. The correlations are determined from the data during 2001–2019. Positive (negative) lags indicate that the FC transport leads [lags] the satellite η in (a) or the tide gauge η leads [lags] the satellite η in (b). Solid (dashed) contours in (a) mark $r = 0.05$ [$r = -0.05$].

subseasonal variability in the FC transport. Given its weak correlation with local winds, the FC transport likely derives most of its subseasonal energy from remote processes.

Mesoscale eddies from the open ocean east of the Bahamas at 26.5°E are a likely remote source of subseasonal variability in the Florida Straits. Frajka-Williams et al. (2013) showed a degree of covariance between the fluctuations of the Antilles Current, a northward flowing current offshore of the Bahamas (e.g., Johns et al., 2008), and the FC transport on timescales longer than 50 days. Based on observations during 2004–2011, they argued that the co-variability between the two western intensified currents was most pronounced for part of the records from mid-2009 to mid-2011 and associated with eddy activity east of the Bahama islands.

We reevaluated the connection between mesoscale eddies and subseasonal variability in the Florida Straits using observations during 2001–2019, with satellite η along 26.5°N east of the Bahamas used as a proxy of eddy activity. The longitude-time plot of the correlation coefficient values between the subseasonal variations of the FC transport and the η for the whole records exhibits an overall weak correlation ($|r| < 0.1$) with a clear westward propagation pattern (Figure 5a). Note a positive correlation value suggests that elevated η associated with anticyclonic eddies east of the Bahamas corresponds with increased FC transport and vice versa.

Although the entire length of the subseasonal data of the FC transport and the η east of the Bahamas shows an overall insignificant correlation, the two parameters are significantly coherent for periods longer than 60 days. The magnitude-squared coherence between the FC transport and the η at 76.9°W for the period band of 60–100 days is 0.56 on average, with a mean phase offset indicative of the transport lagging the sea level by 8 days. Thus, mesoscale eddies potentially account for a substantial fraction of the total variance in the FC transport for the 60–100-day band. Nevertheless, the coherent signals with a phase offset favorable for a plausible eddy-FC causal relationship occur sporadically. Their signatures were strong during 2011, from May to November 2013, and between August 2014–August 2015, while substantially weaker for the rest of the observational period (not shown). The non-stationary nature of the coherent signals might partly explain the overall insignificant correlation between the FC transport and the sea level at 26.5°W east of the Bahama islands on the subseasonal timescale for reasons that remain unclear. In principle, our results are similar to those of Frajka-Williams et al. (2013).

In addition to eddies, baroclinic Rossby waves emanating from the interior of the North Atlantic at a band of latitudes between 27 and 40°N have been reported as a source of the FC variability, particularly for seasonal and longer variations (e.g., Calafat et al., 2018; Domingues et al., 2016). Once impinging upon the U.S. East Coast, the large and low-frequency waves partially turn into coastal-trapped waves, whose energy penetrates the Florida Straits and perturbs the mean flow therein (e.g., Domingues et al., 2016; Huthnance, 2004).

To test whether long Rossby wave signals from the interior affect coastal sea level on the subseasonal timescale, we analyzed the subseasonal variations of satellite η at different longitudes within a band of latitudes between 35 and 37°N and tide gauge η at Duck Pier (36°N). Overall, the subseasonal variations do not demonstrate a lagged correlation pattern indicative of Rossby waves as a facilitator connecting subseasonal signals in the open ocean
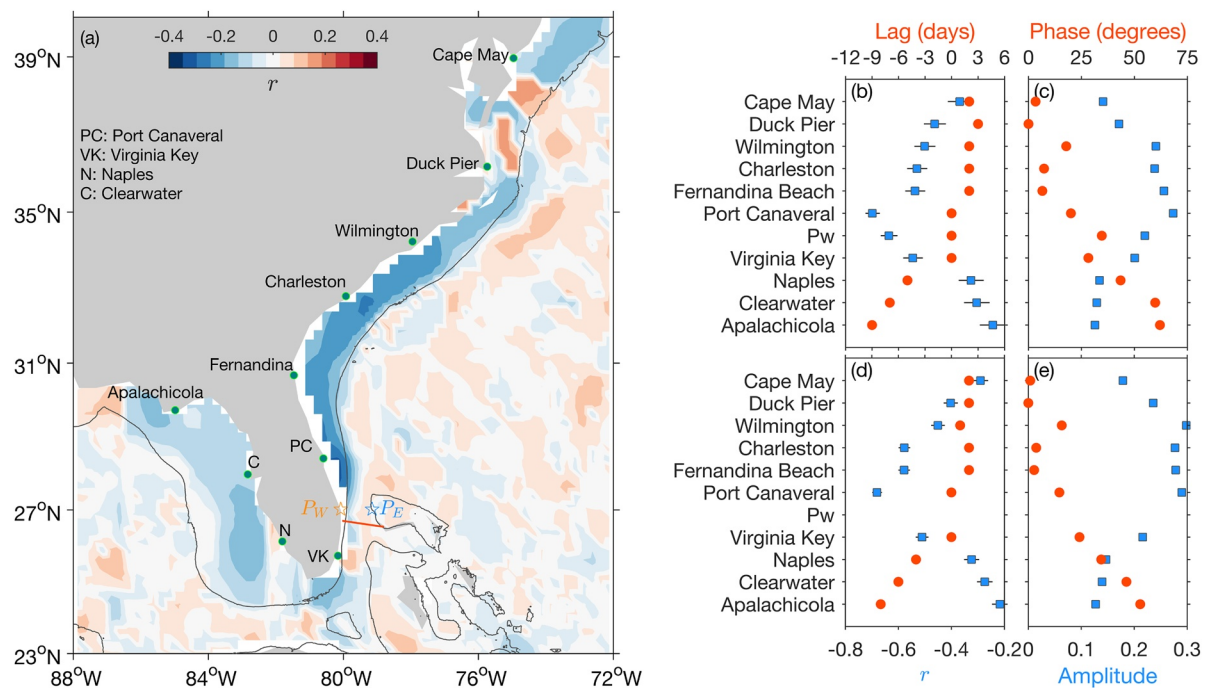
Figure 6. (a) The maximum cross-correlation coefficient between the subseasonal variations of the FC transport and satellite η during 2001–2019 at the lags between −50 and +50 days. The solid contours mark the 200-m isobath. (b) Lagged correlation coefficients, r (boxes), and time lags [circles] between the subseasonal variations of the FC transport and the merged data consisting of the η data observed at tide gauges (shown as green dots in (a)) and the P_W data during July 2008–September 2014. (c) Amplitude (boxes) and phase (circles) of the leading Complex Empirical Orthogonal Function mode of the subseasonal variations of the merged data. (d, e) As in (b, c) but for the subseasonal variations of the FC transport and tide gauge η data during 2001–2019. Each r value in (b, d) is the maximum correlation coefficient value identifiable at the lags between −50 and +50 days. The horizontal lines in (b, d) indicate the 95% bootstrap confidence limits of r.

and along the U.S. East and Gulf Coast. Instead of a pattern indicative of continuous westward propagation from the interior to the coast expected from Rossby waves, the lagged correlation shows a complex pattern of zonal propagation (Figure 5b). Between the coast and 70°E, it is strongest with a slanted pattern to the east, suggesting an eastward phase propagation. The observed eastward phase propagation is likely a zonal projection of subseasonal eddy motions advected by the Gulf Stream. Westward transmissions expected from Rossby waves are a dominant feature to the east of 70°E instead. Thus, it seems that the role of open ocean signals in the subseasonal variability in the FC is of secondary importance.

4. Subseasonal Coastal-Trapped Waves

4.1. Sea Level Versus Florida Current Transport

The overall weak correlation between the FC volume transport and local winds and sea level in the interior suggests remote forcing along the coast as a source of the observed subseasonal variability in the Florida Straits. We first examined η within the continental shelf region along the U.S. East and Gulf Coast to identify a plausible remote driver.

On the 20–100 days period band, the largest correlation between the FC transport and η appears to be confined within the continental shelf of the South Atlantic Bight, with the outer shelf edge marked by an isobath of 200 m (Figure 6a). An inverse relationship pattern between the FC transport and satellite η appears relatively continuous across the continental shelf between Duck Pier and P_W in the Florida Straits. It corroborates the observed relationship between the FC transport and the bottom pressure P_W on the subseasonal period band. However, the inverse correlation between Duck Pier—Cape May and Virginia Key—Clearwater is patchy. It is also apparent that the anti-correlation becomes weaker from Port Canaveral to Virginia Key, particularly in the vicinity of the cable site, which coincides with the narrow continental shelf. What accounts for the patchiness and weak correlation is unknown. Limitations of the gridded altimetry product in resolving η over a narrow shelf and channel, such as the Florida Straits, might contribute to the patchiness.

A merged data of coastal sea level anomaly at tide gauges from Cape May to Apalachicola and P_W during July 2008–September 2014 demonstrates a continuous inverse relationship with the FC transport on the subseasonal timescale (boxes in Figure 6b). The absolute value of the time-lagged correlation coefficients between the FC transport and the merged data for the subseasonal period band is maximum at Port Canaveral ($r \sim 0.7$), within the error limits of the maximum correlation between P_W and the FC transport. Likewise, the correlations between the FC transport and the tide gauge η data extending for the whole records during 2001–2019 show a similar pattern (boxes in Figure 6d). The correlations are more robust for a narrower subseasonal band of 30–40 days, with r about 0.8 at Port Canaveral.

On the subseasonal timescale, the FC transport lags the coastal η data at tide gauges north of the cable. However, it leads those south, indicating propagation into the Gulf of Mexico (red circles in Figures 6b and 6d). It takes about two to 3 days for subseasonal signals to propagate from Cape May to the Florida Straits and about 9 days more to reach Apalachicola. Note that the time lags change little along the Carolina Coast compared to that along the Gulf Coast. Despite being statistically significant (p values are smaller than the significance level), the correlation at other tide gauges north of Cape May and west of Apalachicola is weaker ($r < 0.2$; not shown). Thus, the rest of the analysis is focused on the coastal η data at the tide gauges between Cape May and Apalachicola.

A CEOF analysis of the subseasonal component of the merged P_W and tide gauge η data during July 2008 - September 2014 indicates that the leading CEOF mode of the η data accounts for 61% of the subseasonal variance. The amplitude of the CEOF mode generally increases southward from Cape May to Port Canaveral and then decreases in the Florida Straits and along the U.S. Gulf Coast (boxes in Figure 6c). It captures propagation of subseasonal η as its phase generally increases toward the Gulf of Mexico, indicative of the subseasonal mode first appearing along the U.S. East Coast before reaching the Gulf Coast, via the Florida Straits (circles in Figure 6c). Moreover, the principal component of the CEOF mode is inversely correlated with the subseasonal time series of the FC transport, with a maximum absolute value of r of 0.8. Thus, a linear relationship between the two likely accounts for over 60% of the subseasonal variance of the FC transport. The results do not change when a similar analysis is applied to the subseasonal variations of the tide gauge η only between 2001 and 2019 (Figure 6e).

Like the subseasonal variations of the FC transport and the bottom pressure in the Florida Straits, those in the tide gauge η between Cape May and Apalachicola reveal a seasonal pattern. The standard deviation of the principal component of the leading CEOF mode is the largest on average in October (Figure 3c). Together with other results discussed above, the seasonality of subseasonal η provides another indicator of a relationship between the subseasonal coastal-trapped waves and the FC transport.

4.2. Properties of Subseasonal Coastal Trapped Waves

As discussed above, the FC transport shows a statistically significant correlation with coastal sea level anomaly for the subseasonal period band, particularly between Cape May and Apalachicola, with the corresponding time lag suggestive of along the coast propagation into the Gulf of Mexico. Further analysis of the coastal η data indicates that the propagating feature can be interpreted in terms of coastally trapped wave properties. A wave inference we deduced is the dispersion relation, which was obtained from a coherence analysis of the η data from multiple pairs of tide gauges separated by a distance (d) along the coast, resulting in a set of coherence amplitude and phase (α) estimates at a discrete set of frequencies (ω). Considering only the phase information when the respective coherence amplitude exceeds the 95% significance level, we determined the horizontal wavenumber as $l(\omega) = \frac{\alpha(\omega)}{d}$ for the subseasonal frequency band and subsequently the horizontal dispersion relation, $\omega - l$, with positive l values denoting the horizontal wavenumber along the U.S. East and Gulf Coast in the cyclonic sense of coastal Kelvin wave propagation.

The observed $\omega - l$ values cluster in the first quadrant (most l values > 0), confirming predominant propagation into the Gulf of Mexico on the subseasonal timescale (Figure 7). On average, the ω and l pairs infer a phase speed (ω/l) of 3.8 ± 0.9 m s^{-1} (black dot in Figure 7). Interestingly, the dispersion diagrams of the tide gauge η data along the U.S. East Coast yield a faster phase speed estimate than those along the Gulf Coast. For example, the dispersion diagram derived from the η data at the Duck Pier and Virginia Key pair yields a mean phase speed estimate of 5.8 m s^{-1}, over two times larger than that inferred from the Virginia Key - Apalachicola pair. The cause of the disparity in phase speeds is unclear. However, the shelf width variation along the U.S. East and Gulf Coast, relatively narrower along the South Atlantic Bight coast than along the Gulf Coast of Florida, may play a role in determining the discrepancy.
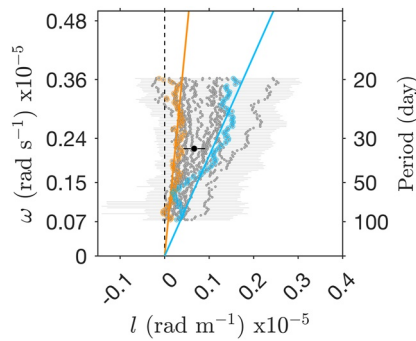
Figure 7. Observed frequency−wavenumber pairs (gray dots; $\omega-l$) for the subseasonal period band, inferred from a coherence analysis of η at tide gauges (green dots in Figure 6a). Positive values of l indicate phase propagation toward the Gulf of Mexico. Orange and blue circles show the dispersion diagram determined from η at Duck Pier and Charleston and η at Port Canaveral and Naples, respectively. The black dot and horizontal line denote the mean and standard deviation values of the observed $\omega-l$ pairs. The orange line demonstrates the theoretical dispersion curve for the first mode of continental shelf wave, while the blue line is for the Kelvin wave. Shades indicate the 95% confidence interval based on a Monte Carlo simulation.

Of several coastal-trapped waveforms that could sustain transmission of subseasonal pulses toward the Gulf of Mexico, continental shelf waves and Kelvin waves are plausible candidates. Considering the significant correlation between the FC transport and η across the shelf region (Figure 6a), particularly on the South Atlantic Bight coast, the shelf waves may account for the observed subseasonal variations. Near the cable site in the Florida Straits, where the cross-strait bathymetric structure is reminiscent of a channel, coastal-trapped waves likely exhibit Kelvin wave characteristics. For example, the dispersion diagram determined from the tide gauge η data at Duck Pier and Charleston (orange circles in Figure 7) appears in good agreement with the theoretical dispersion curve for continental shelf waves (orange line in Figure 7), whose dispersion relation for the wave first mode can be represented as (Schulz et al., 2012)

$$\omega = \frac{L}{\mu + \left(\frac{L}{L_s}\right)^2} l, \tag{1}$$

where L (125 km) is the shelf width, L_s (259 km) is the Rossby radius at the shelf break, and μ (0.88) is an eigenvalue. The observed and theoretical $\omega-l$ result in a similar phase speed of 9 m s^{-1}. The inputs for Equation 1 were determined from the cross-shelf bathymetric profile extending from the tide gauge at Wilmington, a midway between Duck Pier and Charleston, using a method detailed in Schulz et al. (2012).

On the other hand, the theoretical dispersion curve for Kelvin waves whose dispersion relation in the alongshore direction can be represented from theory as

$$\omega = c\, l, \tag{2}$$

yields a slower phase speed of 7.7 m s^{-1} between Duck Pier and Charleston, with c denoting Kelvin wave phase speed. Thus, continental shelf wave dynamics likely account for the subseasonal mode along the Carolina Coast. The Kelvin wave dispersion relation reasonably approximates the observations in the Florida Straits. The observed $\omega-l$ data from η at Port Canaveral and Naples (blue circles in Figure 7) scatter around the Kelvin wave dispersion diagram with $c = 2.1 \pm 0.3$ m s^{-1} (blue line in Figure 7). Of course, due to the actual sloping shelf region, the observed subseasonal waves are not pure coastal Kelvin waves which theoretically require a vertical sidewall. The agreement suggests much smaller shelf-width scales than the baroclinic Rossby deformation radius, whereby a condition of the vertical side boundary for Kelvin waves is applicable.

To gauge whether a vertical sidewall approximation is justified, we determined the ratio of the Rossby deformation radius over the cross-shelf scale of the topography, which can be approximately given as the Burger number

$$Bu = \left(\frac{NH}{\Omega L}\right)^2, \tag{3}$$

where N is the Brunt-Väisällä or buoyancy frequency, H is the vertical scale, Ω is the Coriolis parameter, and L is the cross-shelf length scale (Cushman-Roisin & Beckers, 2011). The cross-shelf length scale is expressed as $L = h/|s|$, where h is the depth of the bottom topography and s is the offshore slope of h. Based on CTD and XBT measurements and bottom topography data in the Florida Straits at 27°N, we argue that most Burger number estimates exceed one (Figure 8). It substantiates that the off-shelf scale of a waveform propagating along the Florida coast follows that of the Rossby deformation radius and is larger than the cross-shelf length scale such
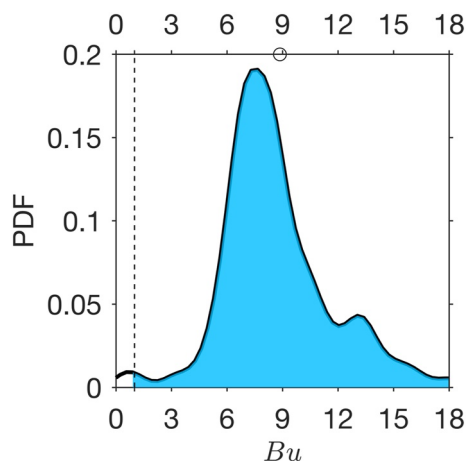
Figure 8. Distribution of the Burger number [Bu] values determined from the hydrographic and bathymetric data at the CTD and XBT stations in the Florida Straits at 27°N during 2001–2019. Shaded area indicates values of $Bu > 1$, and the circle marks the average Bu value.
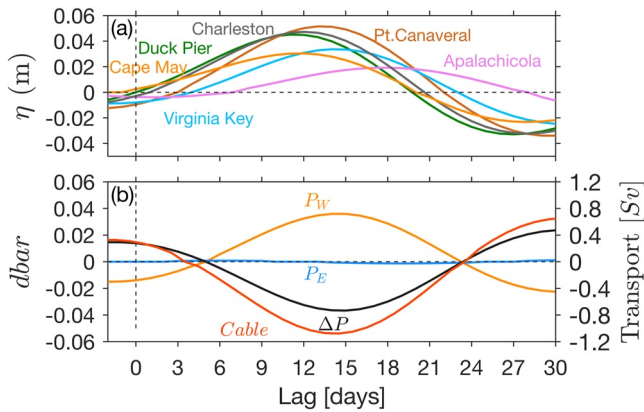
Figure 9. Time-evolution of the subseasonal time series of (a) coastal η at some select tide gauges along the U.S. East and Gulf Coast and (b) the FC transport (red curve) and bottom pressure in the Florida Straits, regressed against the principal component of the leading Complex Empirical Orthogonal Function mode of the subseasonal coastal η data at tide gauges shown in Figure 6a. The regressed time series are scaled to one standard deviation of the principal component. Lag 0 marks when $\eta = 0$ and the rate of change of η is positive at Duck Pier.

that the wave may perceive the continental shelf and slope as a near-vertical sidewall.

The observed stratification frequency in the Florida Straits could provide insight into the phase speeds expected from Kelvin waves. For a given N, solving each baroclinic mode-n Kelvin wave $\frac{\partial}{\partial z}\left(\frac{1}{N^2}\frac{\partial \psi_n}{\partial z}\right) = \frac{\psi_n}{c_n^2}$ as an eigenvalue problem results in the separation constant (c_n) and ψ_n for each mode, with ψ_n denoting the mode-n vertical structure function. Using the N profiles from the hydrographic observations in the Florida Straits at 27°N, the c estimates for the first three gravest baroclinic modes are 1.8 ± 0.2 m s^{-1}, 0.8 ± 0.2 m s^{-1}, and 0.5 ± 0.2 m s^{-1}, respectively. The stratification-derived c estimate for the first baroclinic Kelvin wave mode is within the error limits of the c estimate for the $\omega - l$ diagram inferred from the η data at Port Canaveral and Naples (Figure 7).

To further highlight the evolution, transmission, and impact of subseasonal coastal-trapped waves, we applied a regression analysis between the leading complex principal component and the subseasonal variations of the tide gauge η and the FC transport and bottom pressure in the Florida Straits (Figure 9). The regressed η attributed to a positive one standard deviation of the principal component clearly illustrates the propagation of a coastal-trapped wave crest from the U.S. East Coast to the Gulf Coast (Figure 9a). The wave peak transmits from Duck Pier to Virginia Key within three and a half days, covering a distance of about 1,500 km, equivalent to a wave phase speed of 5.8 m s^{-1}. Along the West Florida Shelf coast from Virginia Key to Apalachicola, with a shorter distance of roughly 970 km between the two tide gauges, it propagates with a slower phase speed of 2.8 m s^{-1}. The phase speeds approximate those derived from the observed dispersion relation (Figure 7).

Besides transmission, the regressed η showcases the evolution of the amplitude of subseasonal coastal-trapped waves as they transmit toward the U.S. Gulf Coast. The wave peak amplitude is up to 5 cm at Port Canaveral. It gradually decays to 2 cm at Apalachicola as the wave propagates into the Gulf of Mexico (Figure 9a). Farther west along the Gulf Coast, the wave amplitude is further attenuated and not different from zero at Port Isabel at the Texas Gulf Coast (not shown).

In the Florida Straits, subseasonal coastal trapped wave crests reduce the cross-stream pressure gradient and the FC transport by up to 0.04 dbar (4 cm) and 1 Sv, respectively (Figure 9b). On the contrary, the subseasonal wave troughs increase the transport and pressure gradient. The pressure gradient - FC transport relationship is similar to that reported by Volkov et al. (2020), who determined a 4 cm/Sv relation, with the sea surface height tilt inferred from altimetry. Our result, however, differs from that obtained by Park and Sweet (2015) and Sweet et al. (2016), who derived a relation of 1.4 cm/Sv. The cause for the discrepancy is unclear, but a barotropic flow assumption used to determine the relation might contribute to their smaller estimate of the sea level gradient across the Florida Straits.

The change in P_W controls the pressure gradient response to subseasonal wave passage in the Florida Straits (Figure 9b). In contrast, P_E shows a lack of change. A more pronounced response in P_W than in P_E may reflect the wave's narrow cross-strait scale relative to the distance between the two pressure recorders. The theoretical Kelvin wave solution for southward moving coastal-trapped waves in the Florida Straits at 27°N signifies a zonal structure of pressure that exponentially decays with distance to the east. It can be presented as

$$P(x) = P_0 e^{\frac{-fx}{c}} \cos(ly - \omega t),$$

where x and y indicate the distance in the cross- and along-strait direction, respectively, and P_0 is the pressure at $x = 0$ or the westernmost of the Florida Straits. Given $x = 80$ km (the nominal zonal distance between the BPRs), $c = 1.8$ m s^{-1} (the phase speed of the first baroclinic Kelvin wave mode estimated from a normal mode decomposition of the observed stratification at 27°N), and assume $P_0 = P_W$, the estimated P_E is a twentieth of P_W. Thus, the insignificant change observed in P_E (blue curve in Figure 9b) may reflect the cross-strait structure of the Kelvin wave, with a decay scale a third of the width of the Florida Straits at 27°N.
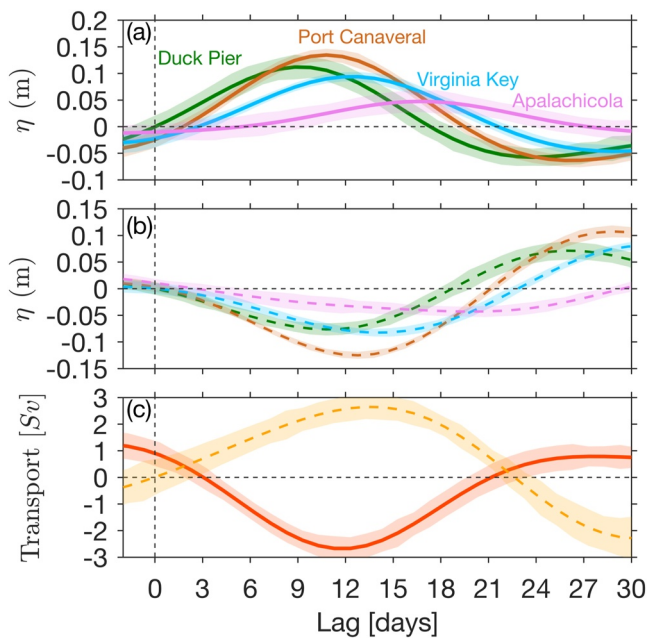
Figure 10. Composites of the subseasonal variations of (a, b) tide gauge η and (c) the FC transport attributed to the extreme subseasonal coastal-trapped wave events during 2001–2019. Solid curves illustrate the composites for the extreme downwelling wave events, while dashed curves demonstrate the composites for the upwelling events. The timing at each location has been lagged at a certain number of days so that Lag 0 marks when $\eta = 0$ and the rate of change of η is positive at Duck Pier. Shading marks the 95% bootstrap confidence limits.

To assess changes to coastal η and the FC transport due to more energetic subseasonal coastal-trapped waves, we defined the principal component values above and lower than the +2 and −2 standard deviation values as extreme events. There are 32 peaks for the positive standard deviation threshold value and 21 troughs for the negative threshold throughout the observation. Henceforth, the peaks are referred to as downwelling events, while the troughs are referred to as upwelling events. It is interesting to note that downwelling events occurred more frequently than upwelling ones for unknown reasons.

Composites of the subseasonal η data associated with the extreme events indicate that subseasonal coastal-trapped waves may modulate sea level anomaly along the South Atlantic Bight coast, with an average amplitude varying between 10 and 15 cm for the downwelling events and 5–10 cm for the upwelling events, respectively (Figures 10a and 10b). The wave crest or trough cycle is about 35 days at each tide gauge. In response to the extreme subseasonal waves, the FC transport registers an average change of 2.6 Sv for the downwelling and upwelling events, respectively (Figure 10c).

5. Basin-Scale Changes Concurrent With Subseasonal Coastal-Trapped Waves

In-situ observations reveal the main characteristics of subseasonal variability in the Florida Straits and along the U.S. East and Gulf Coast. The observations also provide insights into coastal-trapped waves as an energy source for the subseasonal variability. To probe plausible generating mechanisms of the subseasonal waves, we next regress the subseasonal satellite-derived atmospheric and oceanic parameters onto the principal component of the leading CEOF mode of the subseasonal tide gauge η data.

Based on regressed τ, it appears that the observed subseasonal coastal-trapped waves are a transient response to a change in the prevailing subseasonal wind field over the continental shelf region. An initial pattern of suppressed η turns into an elevated η pattern following an alongshore wind reversal from southwesterly to northeasterly roughly along the southern Mid-Atlantic Bight and Carolina Coasts (Figures 11a–11c).

The southwesterly coastal τ is part of a subseasonal anticyclonic wind field over the interior of the subtropical North Atlantic (Figure 12a). At lag 0, while subseasonal sea level anomaly along the U.S. East and Gulf Coast is suppressed, the subseasonal wind is either northeasterly parallel with or into the coast, a wind condition that is not favorable for the suppressed η (Figure 11b). Within the next 2 days, the northeasterly winds build up along the coast extending from Cape May to Fernandina beach and lead to areas of Ekman transport convergence off the coast, which coincide with the emergence of elevated η (Figure 11c). As the winds intensify, subseasonal sea level anomaly continues to increase as well as propagate equatorward along the coast through the next couple of days (Figures 11d–11f). The intensification of the northeasterly coincides with the weakening of the anticyclonic wind over the interior (Figures 12b–12d).

Since the dominant subseasonal mode of the tide gauge η along the South Atlantic Bight and Florida Gulf Coasts is correlated to changes in the basin-scale wind field (Figure 12), the subtropical North Atlantic MOC components at 26.5°N observed by the RAPID/MOCHA/WBTS array demonstrate marked changes coinciding with the subseasonal coastal-trapped wave events. For the downwelling subseasonal wave events, the composite of the Ekman transport component of the MOC shows negative anomalies (blue curve in Figure 13a) or southward Ekman transport at 26.5°N, concurrent with the subseasonal cyclonic wind anomalies prevailing over the ocean interior within subtropical latitudes (a negative anomaly indicates a reduction in the Ekman flow whose long-term average is positive or northward). Compared to the FC transport, the subseasonal variation of the Ekman transport attains its maximum southward transport anomaly of 1.5 Sv a couple of days prior. The offset likely indicates that the observed subseasonal variability in the FC transport, unlike in the Ekman transport, is more of an indirect response to subseasonal changes of the subtropical anticyclone.
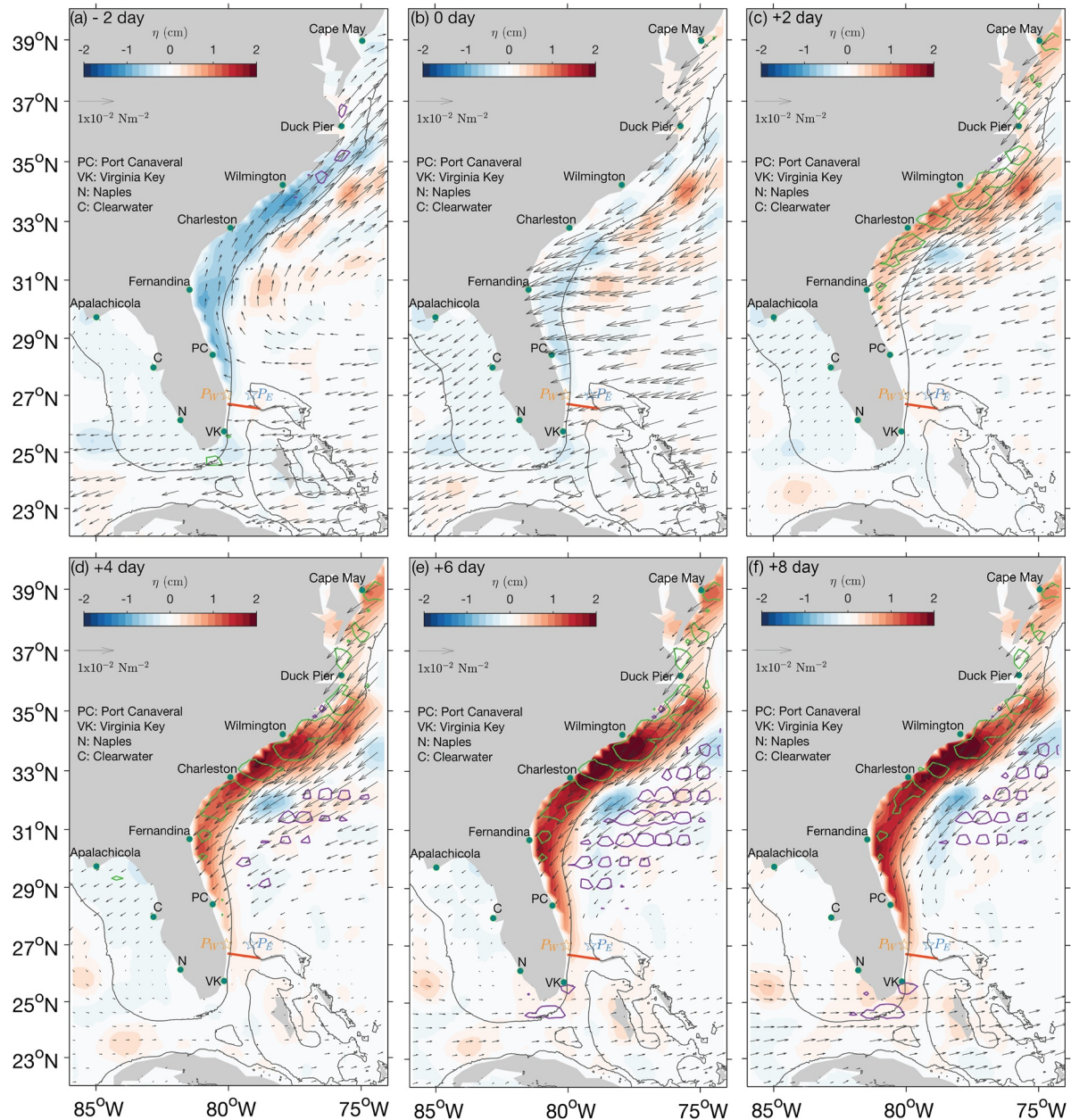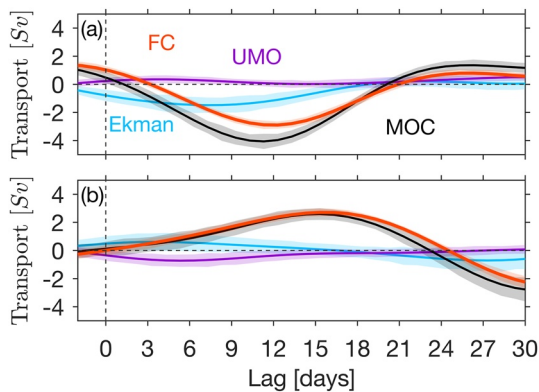
Figure 11. Time-evolution of the subseasonal variations of η (color shading), wind stress (arrows), and Ekman convergence (green contours) and divergence (violet contours), regressed against the principal component of the leading Complex Empirical Orthogonal Function mode of the coastal η data at tide gauges (green dots) along the U.S. East and Gulf Coast. The regressed values are scaled to one standard deviation of the principal component. Omitted values do not exceed the 95% significance level. Green contours denote a value of -10^{-5} m s^{-1}, while the violet ones indicate the opposite sign. Black contours indicate an isobath of 200 m.

While the Ekman transport is southward for the subseasonal downwelling wave events, the UMO transport anomalies are weakly positive with a maximum transport of about 0.4 Sv (magenta curve in Figure 13a). Note that a positive UMO anomaly suggests a reduction in the southward UMO transport. The UMO and Ekman transport anomalies are out of phase, although the former exhibits smaller magnitudes than the latter. The out-of-phase relation might suggest compensation between the two MOC components. A reduction in the northward Ekman transport is partly offset by a reduction in the southward UMO and vice versa. Overall, the northward MOC transport is reduced by up to 4 Sv through the subseasonal downwelling wave events (black curve in Figure 13a), following a reduction in the FC, Ekman, and UMO transports. For the upwelling events, the opposite holds (Figure 13b).
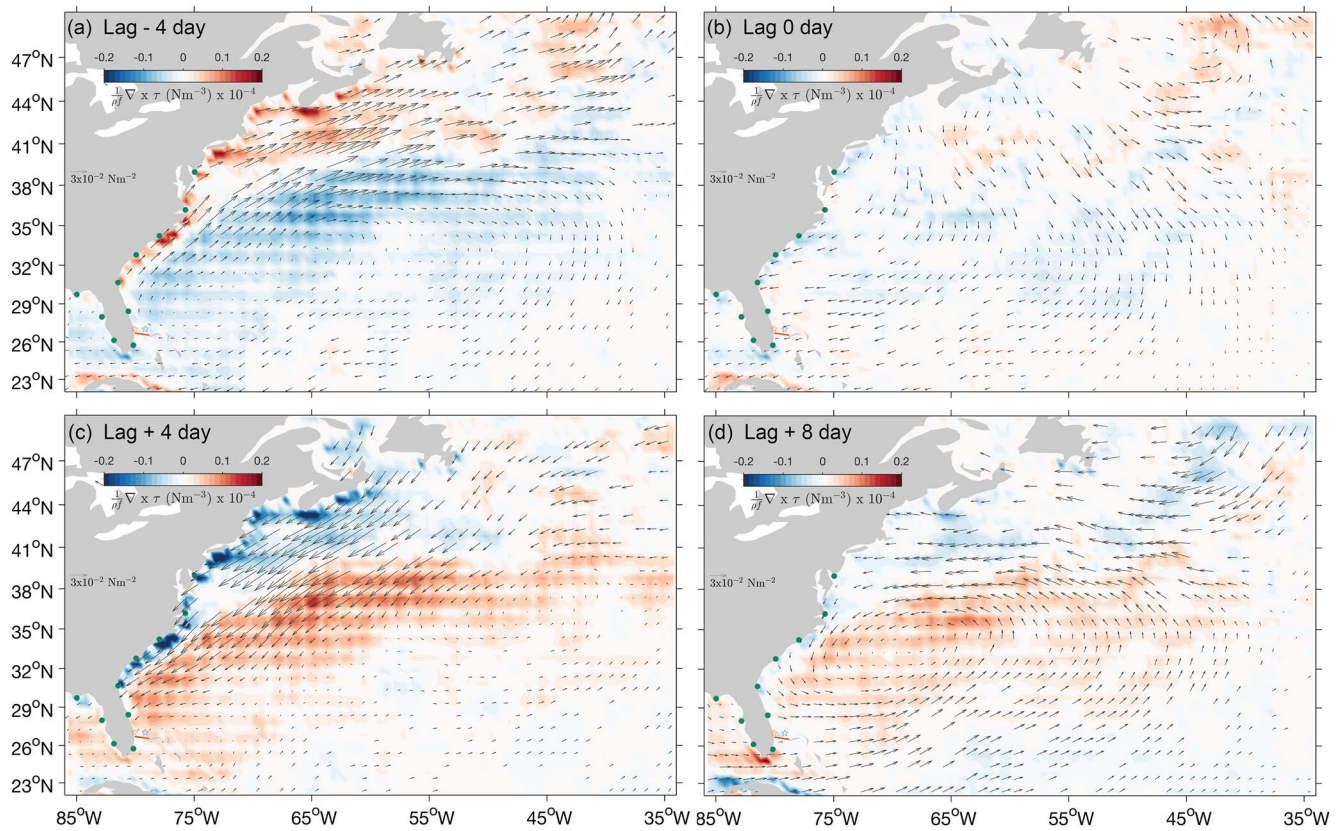
Figure 12. Time-evolution of the subseasonal variations of the wind stress (arrows) and Ekman convergence (blue) and divergence (red), regressed against the first principal component of the complex EOF of the subseasonal η data at tide gauge (green dots) along the U.S. East and Gulf Coast. The regressed values are scaled to one standard deviation of the principal component, with omitted values below a 95% significance level.

Figure 13. Composites of the subseasonal variations of the volume transports constituting the meridional overturning circulation (MOC) observed at 26.5°N in the North Atlantic associated with extreme subseasonal coastal-trapped wave events during April 2004 - December 2019. (a) illustrates the composites for the downwelling events, while (b) demonstrates the composites for the upwelling events. There are 25 downwelling and 17 upwelling events during the observational period of the MOC transports. Red indicates the FC transport, blue denotes the Ekman transport, magenta shows the upper mid-ocean transport, and black demonstrates the MOC transport. As in Figure 10, the timing at each location has been lagged at a certain number of days that Lag 0 marks when $\eta = 0$ and the rate of change of η is positive at Duck Pier. Shading marks the 95% bootstrap confidence limits.

6. Discussion

We have described the main characteristics and plausible mechanisms of the energetic subseasonal variability of the FC volume transport in the Florida Straits. Our observations demonstrate that alongshore wind-forced coastally trapped waves substantially account for the subseasonal variance of the FC transport.

Subseasonal variability constitutes 37% of the total variance of the FC transport, larger than the percentage of the transport synoptic, seasonal, and interannual variances combined. Similar to what is observed in the FC transport, subseasonal variability significantly contributes to the cross-stream pressure gradient changes, with its most robust signature on the west side of the Florida Straits.

The FC transport and the cross-stream pressure gradient are in geostrophic equilibrium on the subseasonal period band, implying that decreased westward pressure gradient corresponds with reduced FC transport and vice versa. The pressure gradient explains 50% of the subseasonal variance in the FC transport by assuming a linear relationship. The percentage increases to 70% when considering the data from September to November only. For comparison, the total pressure gradient variability accounts for about 55% of the total FC transport variance (Meinen et al., 2021).

We argue that the contribution of local wind forcing and open ocean signals to subseasonal variability in the Florida Straits appears to be of secondary

importance. For the whole records during 2001–2019, only up to 5% of the subseasonal variations in the FC transport and local winds covary, with the meridional wind stress component showing the largest covariance. The covariance between the two is sporadic or nonstationary and significant only for some select periods in the subseasonal band, particularly between 20–30 days. Our results are consistent with those reported by Schott et al. (1988). Their study, supported by a frictional model result, suggested that the FC transport and the along-channel wind varying from a few days to a couple of months exhibit a degree of correlation. The correlation is strong mainly for timescales of 15 days and shorter (see Figure 12a of Schott et al. (1988)), consistent with other studies demonstrating coupling between the FC transport and local winds on synoptic timescales, instead of the subseasonal timescales (e.g., Lee & Williams, 1988).

Likewise, the overall impact of mesoscale eddies from east of the Bahamas on the subseasonal variability in the FC transport is not pronounced. The covariance between the subseasonal fluctuations of the FC transport and the eddies is sporadic. The eddies likely govern fewer than 5% of the fluctuations in the FC transport for the full extent of the observations. However, a shorter period in 2011, from May to November 2013 and August 2014–August 2015, shows a stronger correlation between the eddies and FC transport, particularly for the 60–100-day variations. In principle, our results agree with the finding of Frajka-Williams et al. (2013), which reported a nonstationary East Bahama eddies-FC relationship. A plausible mechanism for the nonstationarity is the role of the Antilles Current behaving as a semi-permeable barrier for the eddies (Domingues et al., 2019).

While weakly correlated with local winds and signals from the interior, the subseasonal variability of the FC transport exhibits a stronger correlation with the coastal sea level anomaly between Cape May and Apalachicola along the U.S. East and Gulf Coast. The correlation is maximum at Port Canaveral ($r \sim 0.7$) and indicates propagating subseasonal signals toward the Gulf Coast. About 61% of the subseasonal variance of the tide gauge η data signifies coastal-trapped waves. They likely account for over 60% of the subseasonal variability in the FC transport.

When regressed against the principal component of the leading CEOF mode of the subseasonal variability of the tide gauge data, η illustrates the spatial and temporal changes of coastal-trapped waves. The regressed η at different tide gauges shows transmission of the subseasonal waves covering a wave path between Cape May and Apalachicola within 8 days, with the waves traveling faster along the U.S. East Coast. For example, the wave phase speed is 5.8 m s^{-1} between Duck Pier and Virginia Key along the South Atlantic Bight coast, while 2.8 m s^{-1} between Virginia Key and Apalachicola along the Gulf Coast of Florida. The phase speed is particularly fast along the Carolina coast. The observations at Duck Pier and Charleston show that the subseasonal mode is likely in the form of continental shelf waves propagating at an average speed of 9 m s^{-1}. A wider continental shelf along the Gulf coast of Florida might play a role in a phase speed decrease. Schulz et al. (2012) argued that continental shelf waves behave as topographic Rossby waves and propagate slower on wide shelves.

In the Florida Straits, particularly in the proximity of the cable site at 27°N, subseasonal coastal-trapped waves could be in the form of Kelvin waves and markedly affect the FC transport. The regressed η and FC transport show that a subseasonal coastal-trapped wave pulse with an amplitude of 5 cm at Port Canaveral exerts a 1 Sv change in the FC transport. The average wave amplitude could be as high as 15 cm for extreme cases, and it may modulate the FC transport on average by 2.6 Sv. We note that the average amplitude of the extreme subseasonal waves is commensurate with the global average sea-level rise over the 20th century of about 16 cm (Calafat et al., 2018).

A geostrophic balance between the FC transport and the cross-stream pressure gradient or east-west pressure difference is evident during subseasonal wave passage, with P_W controlling the pressure gradient change. The minimum P_E response appears consistent with the zonal structure of the Kelvin wave pressure, which decays away from the Florida coast with a scale of about 27 km in the Florida Straits. Mooers et al. (2005) reported a similar decay scale of 25 km inferred from the zonal structure of the model FC throughout an intense cold front-forced coastal trapped wave event in the Florida Straits.

The stratification frequency and bottom topography across the Florida Straits at 27°N indicate that the properties of Kelvin waves may explain the observed subseasonal coastal-trapped waves therein. A normal mode decomposition of the buoyancy frequency yields a phase speed of 1.8 m s^{-1} for the first baroclinic Kelvin wave mode, similar to that inferred from the observed dispersion diagram obtained from η at Port Canaveral and Naples. Moreover, the baroclinic Rossby deformation radius is, on average, nine times the cross-shelf scale of

the bottom topography along 27°N in the Florida Straits, implying a Kelvin wave prerequisite of near-vertical sidewall condition.

Subseasonal coastal-trapped wave energy substantially dissipates along the Gulf of Mexico coast. The regressed coastal η indicates that the observed subseasonal wave amplitude rapidly decreases between the Florida Straits and Apalachicola. Determining the root cause of the wave damping is beyond the scope of this study, but interactions with coastal and bottom topography and background mean flow might be a factor. As subseasonal waves propagate equatorward against strong background currents, such as the Gulf Stream and Loop Current, and along complex coastal curvatures with variable cross-stream bottom topography, wave energy attenuation is expected.

Low-frequency oceanic Rossby waves from the eastern North Atlantic are not the main contributor to the dynamic origins of the observed subseasonal coastal-trapped waves in the Florida Straits. Instead, Ekman dynamics along-shore of the northern South Atlantic Bight may account for the genesis of the subseasonal waves. The emergence of subseasonal alongshore winds off the New Jersey coast and, subsequently, the Carolina coast precedes the onset of the subseasonal mode. Against the background wind field of the subtropical high, the Ekman convergence-favorable northeasterly winds induce elevated coastal η off Cape May on the subseasonal times-cales. Conversely, the opposite holds for the Ekman divergence-favorable southeasterly winds. The perturbed sea level anomaly progresses toward the Gulf of Mexico as a train of subseasonal coastal-trapped waves, modulating coastal sea level anomaly along the wave path and the Florida Current transport in the Florida Straits. While the subseasonal coastal trapped waves propagating along the Florida East and Gulf Coasts likely behave as a free wave, it remains unclear whether the subseasonal waves traversing along the Carolina Coast are independent of the prevailing alongshore winds. Some numerical experiments to further explore the subseasonal waves' genesis and impact on ocean-atmosphere interaction are to be carried out for future studies.

The basin-wide wind field associated with the subseasonal alongshore winds exhibits a vortex-like structure over the subtropical North Atlantic. Time evolution of the regressed subseasonal τ over the North Atlantic illustrates a subtropical anticyclonic circulation that transitions into cyclonic and vice versa before and during the generation of the observed subseasonal coastal-trapped waves. The subseasonal anticyclonic and cyclonic winds might be a subseasonal component of the subtropical anticyclone, typically referred to as the "Azores" or "Bermuda High," part of the global atmospheric circulation (Davis et al., 1997). The subtropical anticyclone attains its minimum intensity in October (Sahsamanoglou, 1990), which coincides with the subseasonal waves' most energetic period as observed in the tide gauge η and FC transport. Davis et al. (1997) ascribe the weakening of the subtropical anti-cyclone through boreal autumn to its high-pressure center's eastward migration (Davis et al., 1997), which shows profound subseasonal variations (Osman et al., 2021). Any plausible interplays between intensified subseasonal wind and suppressed subtropical anticyclone in autumn are to be investigated.

Subseasonal changes of the subtropical high-associated wind impact not only the FC transport but also other components of the MOC transport, particularly the Ekman transport component. Anomalous cyclonic winds over the subtropics, coinciding with the downwelling coastal-trapped wave events that attenuate the FC transport, drive southward Ekman transport anomaly with a maximum magnitude of up to 1.5 Sv across 26.5°N east of the Bahamas. The anomalous winds, however, exert a more subdued impact on the UMO transport, reducing it by a maximum of 0.4 Sv. The reduced UMO transport partly offsets weakened Ekman transport, but it is too small to suggest a compensation between the two components. It is also unlikely to compensate for the FC transport, whose magnitude could be weakened by up to 2.6 Sv during the subseasonal downwelling wave events. As a result, reduced MOC transport by up to about 4 Sv is observed during the downwelling wave events, whereas the opposite holds for the upwelling wave events. Thus, it seems that a degree of compensation between the MOC components reported by previous studies (e.g., Frajka-Williams et al., 2016; Kanzow et al., 2007) is less clear from the subseasonal component of the MOC transports.

7. Conclusions

We evaluated the characteristics and dynamical origins of the FC subseasonal variability between 20 and 100 days from a suite of in-situ and satellite measurements in the Florida Straits and the broader region in the North Atlantic during 2001–2019. Results obtained in this work show that subseasonal variability comprises 37% of the total variance of the FC volume transport. It is energetic through September - November and attains its maximum in October. In addition, we also found that alongshore wind-forced coastal-trapped waves are the primary

mechanism for the subseasonal variations of the FC transport and the sea level anomaly between Cape May and Apalachicola along the U.S. East and Gulf Coast. The role of local winds over the Florida Straits, mesoscale eddies from east of the Bahama islands, and low-frequency Rossby waves from the eastern North Atlantic is of secondary importance on the subseasonal time scale.

Subseasonal coastal-trapped waves complete their cycle in 35 days. They propagate along a coastal waveguide between Cape May and Apalachicola within 8 days, likely as Kelvin waves in the proximity of the cable site in the Florida Straits and as continental shelf waves along the rest of the waveguide, with a mean phase speed of about 4 m s^{-1}. The average amplitude of the subseasonal waves is up to 15 cm at Port Canaveral and rapidly decays as it transmits along the Gulf of Mexico coast.

We infer that the observed subseasonal coastal-trapped waves may exhibit Kelvin wave characteristics in the Florida Straits. First, the observed dispersion diagram signifies a non-dispersive relation for the Kelvin wave. The first baroclinic mode might be the most dominant modal structure of the wave. Second, the wave-induced FC transport change of 1 Sv is in geostrophic balance with the cross-stream pressure difference of about 4 cm. On average, the subseasonal mode may change the FC transport by 2.6 Sv for extreme cases. Third, the cross-stream pressure structure rapidly declines eastward from the Florida coast. It likely decays exponentially with a scale of 27 km, a function of the baroclinic Rossby deformation radius. Fourth, the deformation radius, on average, exceeds the cross-shelf scale by a factor of nine, justifying a vertical sidewall approximation.

The along-shore winds forcing the subseasonal waves are part of subseasonal changes to the subtropical anti-cyclonic winds. The anomalous subseasonal winds over the subtropics drive the Ekman and UMO transport anomalies at 26.5°N by up to 1.5 and 0.4 Sv, respectively. The average MOC transport anomaly associated with the subseasonal winds is up to 4 Sv.

Data Availability Statement

The FC transport estimates from cable voltages and altimetry can be downloaded via www.aoml.noaa.gov/phod/floridacurrent/. The pressure, LADCP, and dropsonde data are available at www.aoml.noaa.gov/phod/wbts/, and the XBT data are archived at https://www.aoml.noaa.gov/phod/goos/xbtscience/data.php. The satellite data can be obtained from http://marine.copernicus.eu/services-portfolio/access-to-products. The MOC transports are from https://rapid.ac.uk/rapidmoc/rapid_data/transports.php.

References

Baringer, M. O. N., & Larsen, J. C. (2001). Sixteen years of Florida Current transport at 27 N. *Geophysical Research Letters*, *28*(16), 3179–3182. https://doi.org/10.1029/2001gl013246

Beal, L. M., Hummon, J. M., Williams, E., Brown, O. B., Baringer, W., & Kearns, E. J. (2008). Five years of Florida Current structure and transport from the royal Caribbean cruise ship explorer of the seas. *Journal of Geophysical Research*, *113*(C6), C06001. https://doi.org/10.1029/2007jc004154

Calafat, F. M., Wahl, T., Lindsten, F., Williams, J., & Frajka-Williams, E. (2018). Coherent modulation of the sea-level annual cycle in the United States by Atlantic Rossby waves. *Nature Communications*, *9*(1), 1–13. https://doi.org/10.1038/s41467-018-04898-y

Caldwell, P. C., Merrifield, M. A., & Thompson, P. R. (2015). Sea level measured by tide gauges from global oceans—The joint archive for Sea Level holdings (NCEI accession 0019568), version 5.5. Dataset. *NOAA National Centers for Environmental Information*. https://doi.org/10.7289/V5V40S7W

Cushman-Roisin, B., & Beckers, J.-M. (2011). *Introduction to geophysical fluid dynamics: Physical and numerical aspects*. Academic press.

Czeschel, L., Eden, C., & Greatbatch, R. J. (2012). On the driving mechanism of the annual cycle of the Florida Current transport. *Journal of Physical Oceanography*, *42*(5), 824–839. https://doi.org/10.1175/jpo-d-11-0109.1

Davis, R. E., Hayden, B. P., Gay, D. A., Phillips, W. L., & Jones, G. V. (1997). The North Atlantic subtropical anticyclone. *Journal of Climate*, *10*(4), 728–744. https://doi.org/10.1175/1520-0442(1997)010<0728:tnasa>2.0.co;2

DiNezio, P. N., Gramer, L. J., Johns, W. E., Meinen, C. S., & Baringer, M. O. (2009). Observed interannual variability of the Florida Current: Wind forcing and the North Atlantic oscillation. *Journal of Physical Oceanography*, *39*(3), 721–736. https://doi.org/10.1175/2008jpo4001.1

Domingues, R., Baringer, M., & Goni, G. (2016). Remote sources for year-to-year changes in the seasonality of the Florida Current transport. *Journal of Geophysical Research: Oceans*, *121*(10), 7547–7559. https://doi.org/10.1002/2016JC012070

Domingues, R. M., Johns, W. E., & Meinen, C. S. (2019). Mechanisms of eddy-driven variability of the Florida Current. *Journal of Physical Oceanography*, *49*(5), 1319–1338. https://doi.org/10.1175/jpo-d-18-0192.1

Frajka-Williams, E., Ansorge, I. J., Baehr, J., Bryden, H. L., Chidichimo, M. P., Cunningham, S. A., et al. (2019). Atlantic meridional overturning circulation: Observed transport and variability. *Frontiers in Marine Science*, *260*. https://doi.org/10.3389/fmars.2019.00260

Frajka-Williams, E., Johns, W. E., Meinen, C. S., Beal, L. M., & Cunningham, S. A. (2013). Eddy impacts on the Florida Current. *Geophysical Research Letters*, *40*(2), 349–353. https://doi.org/10.1002/grl.50115

Frajka-Williams, E., Meinen, C. S., Johns, W. E., Smeed, D. A., Duchez, A., Lawrence, A. J., et al. (2016). Compensation between meridional flow components of the Atlantic MOC at 26 N. *Ocean Science*, *12*(2), 481–493. https://doi.org/10.5194/os-12-481-2016

Garcia, R. F., & Meinen, C. S. (2014). Accuracy of Florida Current volume transport measurements at 27 N using multiple observational techniques. *Journal of Atmospheric and Oceanic Technology*, *31*(5), 1169–1180. https://doi.org/10.1175/jtech-d-13-00148.1

Grinsted, A., Moore, J. C., & Jevrejeva, S. (2004). Application of the cross wavelet transform and wavelet coherence to geophysical time series. *Nonlinear Processes in Geophysics*, *11*(5/6), 561–566. https://doi.org/10.5194/npg-11-561-2004

Huthnance, J. M. (2004). Ocean-to-shelf signal transmission: A parameter study. *Journal of Geophysical Research*, *109*(C12), C12029. https://doi.org/10.1029/2004JC002358

Johns, W. E., Beal, L. M., Baringer, M. O., Molina, J. R., Cunningham, S. A., Kanzow, T., & Rayner, D. (2008). Variability of shallow and deep western boundary currents off the Bahamas during 2004–05: Results from the 26_N RAPID–MOC array. *Journal of Physical Oceanography*, *38*(3), 605–623. https://doi.org/10.1175/2007jpo3791.1

Johns, W. E., & Schott, F. (1987). Meandering and transport variations of the Florida Current. *Journal of Physical Oceanography*, *17*(8), 1128–1147. https://doi.org/10.1175/1520-0485(1987)017<1128:matvot>2.0.co;2

Kanamitsu, M., Ebisuzaki, W., Woollen, J., Yang, S., Hnilo, J. J., Fiorino, M., & Potter, G. L. (2002). NCEP–DOE AMIP-II reanalysis (R-2). *Bulletin of the American Meteorological Society*, *83*(11), 1631–1644. https://doi.org/10.1175/bams-83-11-1631(2002)083<1631:nar>2.3.co;2

Kanzow, T., Cunningham, S. A., Rayner, D., Hirschi, J. J. M., Johns, W. E., Baringer, M. O., et al. (2007). Observed flow compensation associated with the MOC at 26.5 N in the Atlantic. *Science*, *317*(5840), 938–941. https://doi.org/10.1126/science.1141293

Larsen, J., & Smith, F. (1992). Transport and heat flux of the Florida Current at 27 N derived from cross-stream voltages and profiling data: Theory and observations. *Philosophical Transactions of the Royal Society of London, Series A: Physical and Engineering Sciences*, *338*(1650), 169–236. https://doi.org/10.1098/rsta.1992.0007

Larsen, J. C. (1991). Transport measurements from in-service undersea telephone cables. *IEEE Journal of Oceanic Engineering*, *16*(4), 313–318. https://doi.org/10.1109/48.90893

Lau, W. K.-M., & Waliser, D. E. (2011). *Intraseasonal variability in the atmosphere-ocean climate system*. Springer Science & Business Media.

Lee, T. N., Schott, F. A., & Zantopp, R. (1985). Florida Current: Low-frequency variability as observed with moored current meters during April 1982 to June 1983. *Science*, *227*(4684), 298–302. https://doi.org/10.1126/science.227.4684.298

Lee, T. N., & Williams, E. (1988). Wind-forced transport fluctuations of the Florida Current. *Journal of Physical Oceanography*, *18*(7), 937–946. https://doi.org/10.1175/1520-0485(1988)018<0937:Wftfot>2.0.Co;2

Maloney, E. D., Chelton, D. B., & Esbensen, S. K. (2008). Subseasonal SST variability in the tropical eastern North Pacific during boreal summer. *Journal of Climate*, *21*(17), 4149–4167. https://doi.org/10.1175/2007jcli1856.1

McCarthy, G. D., Smeed, D. A., Johns, W. E., Frajka-Williams, E., Moat, B. I., Rayner, D., et al. (2015). Measuring the Atlantic meridional overturning circulation at 26 N. *Progress in Oceanography*, *130*, 91–111. https://doi.org/10.1016/j.pocean.2014.10.006

Meinen, C. S., Baringer, M. O., & Garcia, R. F. (2010). Florida Current transport variability: An analysis of annual and longer-period signals. *Deep Sea Research Part I: Oceanographic Research Papers*, *57*(7), 835–846. https://doi.org/10.1016/j.dsr.2010.04.001

Meinen, C. S., Smith, R. H., & Garcia, R. F. (2021). Evaluating pressure gauges as a potential future replacement for electromagnetic cable observations of the Florida Current transport at 27 degrees N. *Journal of Operational Oceanography*, *14*(2), 166–176. https://doi.org/10.1080/1755876x.2020.1780757

Mooers, C. N. K., Meinin, C. S., Baringer, M. O., Bang, I., Rhodes, R., Barron, C. N., & Bub, F. (2005). Cross validating ocean prediction and monitoring systems. *Eos, Transactions American Geophysical Union*, *86*(29), 269–273. https://doi.org/10.1029/2005eo290002

Osman, M., Zaitchik, B., Badr, H., & Hameed, S. (2021). North Atlantic centers of action and seasonal to subseasonal temperature variability in Europe and eastern North America. *International Journal of Climatology*, *41*(S1), E1775–E1790. https://doi.org/10.1002/joc.6806

Park, J., & Sweet, W. (2015). Accelerated sea level rise and Florida Current transport. *Ocean Science*, *11*(4), 607–615. https://doi.org/10.5194/os-11-607-2015

Percival, D. B., & Walden, A. T. (1993). *Spectral analysis for physical applications*. Cambridge University Press.

Piecuch, C. G., & Ponte, R. M. (2015). Inverted barometer contributions to recent sea level changes along the northeast coast of North America. *Geophysical Research Letters*, *42*(14), 5918–5925. https://doi.org/10.1002/2015GL064580

Ponte, R. M. (2006). Low-frequency sea level variability and the inverted barometer effect. *Journal of Atmospheric and Oceanic Technology*, *23*(4), 619–629. https://doi.org/10.1175/jtech1864.1

Rosenfeld, L. K., Molinari, R. L., & Leaman, K. D. (1989). Observed and modeled annual cycle of transport in the straits of Florida and east of Abaco-Island, the Bahamas (26.5-degrees-N). *Journal of Geophysical Research*, *94*(C4), 4867–4878. https://doi.org/10.1029/JC094iC04p04867

Sahsamanoglou, H. S. (1990). A contribution to the study of action centres in the North Atlantic. *International Journal of Climatology*, *10*(3), 247–261. https://doi.org/10.1002/joc.3370100303

Schott, F. A., Frisch, S. A., & Larsen, J. C. (1986). Comparison of surface currents measured by HF Doppler radar in the Western Florida straits during November 1983 to January 1984 and Florida Current transports. *Journal of Geophysical Research*, *91*(C7), 8451–8460. https://doi.org/10.1029/JC091iC07p08451

Schott, F. A., Lee, T. N., & Zantopp, R. (1988). Variability of structure and transport of the Florida Current in the period range of days to seasonal. *Journal of Physical Oceanography*, *18*(9), 1209–1230. https://doi.org/10.1175/1520-0485(1988)018<1209:vosato>2.0.co;2

Schulz, W. J., Mied, R. P., & Snow, C. M. (2012). Continental shelf wave propagation in the mid-Atlantic Bight: A general dispersion relation. *Journal of Physical Oceanography*, *42*(4), 558–568. https://doi.org/10.1175/jpo-d-11-098.1

Sweet, W. V., Menendez, M., Genz, A., Obeysekera, J., Park, J., & Marra, J. J. (2016). In tide's way: Southeast Florida's September 2015 sunny-day flood. *Bulletin of the American Meteorological Society*, *97*(12), S25–S30. https://doi.org/10.1175/bams-d-16-0117.1

Thomson, R. E., & Emery, W. J. (2014). Chapter 5—Time series analysis methods. In R. E. Thomson & W. J. Emery (Eds.), *Data analysis methods in physical oceanography* (3rd ed., pp. 425–591). Elsevier. https://doi.org/10.1016/B978-0-12-387782-6.00005-3

Volkov, D. L., Domingues, R., Meinen, C. S., Garcia, R., Baringer, M., Goni, G., & Smith, R. H. (2020). Inferring Florida current volume transport from satellite altimetry. *Journal of Geophysical Research: Oceans*, *125*(12), e2020JC016763. https://doi.org/10.1029/2020JC016763